**Article ID:** 1000-324X(2019)06-0679-06 **DOI:** 10.15541/jim20180528

# Fabrication and Planar Cooling Performance of Flexible $Bi_{0.5}Sb_{1.5}Te_3$/Epoxy Composite Thermoelectric Films

LI Peng, NIE Xiao-Lei, TIAN Ye, FANG Wen-Bing, WEI Ping, ZHU Wan-Ting, SUN Zhi-Gang, ZHANG Qing-Jie, ZHAO Wen-Yu

(State Key Laboratory of Advanced Technology for Materials Synthesis and Processing, Wuhan University of Technology, Wuhan 430070, China)

**Abstract:** Flexible $Bi_{0.5}Sb_{1.5}Te_3$/epoxy composite thermoelectric films were prepared on polyimide substrates by screen printing. Its electrical transport properties are enhanced by optimizing the content of $Bi_{0.5}Sb_{1.5}Te_3$ powder. The highest power factor of the optimized $Bi_{0.5}Sb_{1.5}Te_3$/epoxy films reached 1.12 $mW \cdot m^{-1} \cdot K^{-2}$ at 300 K, increased by 33% as compared with previous value. The anti-bending test results show that resistance of the thick films remains unchanged when the bending radius is over 20 mm and slightly increases within 3000 bending cycles when the bending radius is 20 mm, implying that the as-prepared films have potential application in flexible TE devices. The flexible thermoelectric leg could establish a temperature difference from 4.2 ℃ to 7.8 ℃ under working current from 0.01 A to 0.05 A, showing potential application in planar cooling field.

**Key words:** flexible thermoelectric films; screen printing; $Bi_{0.5}Sb_{1.5}Te_3$/epoxy composite films; electrical property; planar cooling field

Development of microelectronic integrated technology resulted in increase in the heat flux density, which seriously affects the performance and service life of the electronic devices[1-2]. Therefore, how to effectively take away the harmful waste heat poses great challenges. Among various heat dissipation techniques[3], thermoelectric (TE) cooling based on Peltier effect of TE materials has attracted increasing attention due to a series of unique advantages such as no noise, no pollution, no moving parts, rapid cooling, simple operation, high reliability, and lightweight, which is expected to solve the problem of heat dissipation of electronic devices with high heat flux[4-6]. However, most of the commercial TE cooling devices adopt a vertical design, in which the heat flows along the longitudinal direction[7-9]. These TE cooling devices are composed of bulk P and N type thermoelectric legs connected electrically in series through metallic electrodes and then sandwiched between two electrically insulated and thermally conductive ceramic plates. Thus this structure has poor flexibility and is very difficult to realize dimensionally match between TE devices and electronic components[10]. However, the cooling performance deteriorated seriously when the device is downscaled to micro level. While for another type of TE cooling devices using planar design, in which the heat flow is parallel to the substrate, their relatively long TE legs can be fabricated from TE films which are beneficial to flexibility, miniaturization and relatively large temperature difference.

$Bi_2Te_3$–based alloys ($Bi_xSb_{2-x}Te_3$ and $Bi_2Te_{3-x}Se_x$) are customarily regarded as the representative of $V_2VI_3$ TE materials, and have been commercialized and widely used for refrigeration and energy conversion applications in the low-temperature range[11-12]. Although great progress was made in developing bulk $Bi_2Te_3$ materials with high performance, performance of $Bi_2Te_3$–based films is still unsatisfactory. As a simple and efficient process to prepare TE films[13-16], the bottleneck of printing lies in the deterioration of electrical transport properties which results from low density and various structural defects such as holes and cracks[17]. Several strategies were employed to enhance the electrical transport properties of the printed TE films, such as cold isostatic pressing[18-19], addition of sintering aids[20], and high-temperature sintering to remove the insulating binders[21]. However, realization of high-performance flexible TE cooling de-

**Received date:** 2018-11-09; **Modified date:** 2019-01-24
**Foundation item:** National Natural Science Foundation of China (11834012, 51620105014, 51572210, 51521001); National Key Research and Development Plan of China (2018YFB0703600)
**Biography:** LI Peng (1995–), male, candidate of Master degree. E-mail: penglee@whut.edu.cn
**Corresponding author:** NIE Xiao-Lei, laboratory technician. E-mail: xiaoleinie@whut.edu.cn; ZHAO Wen-Yu, professor. E-mail: wyzhao@whut.edu.cn

vices is still frustrated by the poor electrical transport properties.

In previous work[22], $Bi_{0.5}Sb_{1.5}Te_3$/epoxy flexible thick films with (000*l*) preferential orientation were prepared on polyimide substrates by combination of brush-printing and hot-pressing curing processes, which greatly improved the electrical transport properties of the composite thick films. However, brush-printing process is difficult to realize mass production due to its poor controllability. In this work, a series of $Bi_{0.5}Sb_{1.5}Te_3$/epoxy composite flexible thermoelectric thick films were successfully prepared on polyimide substrates by screen printing, and the electrical transport properties of the thick films were further improved by optimizing the content of $Bi_{0.5}Sb_{1.5}Te_3$ powder.

## 1 Experimental

The preparation of thermoelectric slurries refers to the method reported in former work[22]. Thermoelectric slurry was prepared by using diglycidyl ether of bisphenol-F epoxy resin as adhesives, methylhexahydrophthalic anhydride as hardener, 2-ethyl-4-methylimidazole (2E4MI) as anhydride accelerator and $Bi_{0.5}Sb_{1.5}Te_3$ as thermoelectric component. Firstly, $Bi_{0.5}Sb_{1.5}Te_3$ ingots were crushed and pulverized with a planetary ball mill at a speed of 200 r/min for 24 h under the protection of argon, then dried in vacuum oven at 60 ℃ for 2 h to get thermoelectric powder. Secondly, epoxy resin, hardener, catalyst and diluent were mixed to form the epoxy system mixture.

The obtained thermoelectric slurries were printed on the pre-cleaned polyimide (PI) substrates by screen printing to form thick films. The films were dried in vacuum at 100 ℃ for 60 min, and then cured at 300 ℃ for 4 h in hot-pressing apparatus. To further reveal the impact of the content of $Bi_{0.5}Sb_{1.5}Te_3$ on the electrical properties of the composite films, the slurries were prepared with different content of $Bi_{0.5}Sb_{1.5}Te_3$ powder ($x$=6.5, $x$=7, $x$=8, $x$=9 and $x$=10) where $x$ represents the mass ratio of $Bi_{0.5}Sb_{1.5}Te_3$ to epoxy system (epoxy resin, hardener and catalyst).

The phase constituents of all thick films were determined by X-ray diffraction (XRD, PANalytical χ' Pert PRO) using Cu $K_\alpha$ radiation ($\lambda$=0.15418 nm). Microstructures were examined by a field emission scanning electron microscope (FESEM, Zeiss ULTRA-PLUS-43-13). The density of the thick films was measured with the Archimedes method. The Hall coefficient ($R_H$), carrier concentration ($n$), mobility ($\mu_H$) and electrical conductivity ($\sigma$) of the thick films were tested by the HL5500 Hall effect test system at room temperature. The in-plane electrical conductivity ($\sigma$) and Seebeck coefficient ($\alpha$) were measured with the standard four-probe method (Sinkuriko, ZEM-3) in He atmosphere. The measurement error for $\sigma$ and $\alpha$ is ±5%. The bending tests of the thick films were performed using a homemade bending test apparatus. The temperature distribution of the TE leg was measured under different applied currents ($I$) by visual infrared thermometer (FLUKE, TI 400).

## 2 Results and discussion

XRD patterns of these composite films are displayed in Fig. 1. All diffraction peaks can be indexed to the standard diffraction data of $Bi_{0.5}Sb_{1.5}Te_3$ (JCPDS 49-1713), indicating that these films are composed of single-phase $Bi_{0.5}Sb_{1.5}Te_3$.

Fig. 2 shows the cross-sectional FESEM images of these composite films. The thicknesses of these films are approximate 20 μm. It is apparent that there are organic residues and pores in all the films. As the content of $Bi_{0.5}Sb_{1.5}Te_3$ powder increased from $x$=6.5 to $x$=8, the organic residues were reduced. However, with $x$ further increasing, the pores were obviously increased. Thus the film prepared with $x$=8 has the most compact microstructure, which could be also identified from the variation of film densities (Table 1).

The room-temperature electrical transport properties of these composite films are listed in Table 1. The positive Hall coefficient $R_H$ indicated that most of carriers were holes. The p-type conduction character was consistent with the corresponding bulk materials[23]. Variation of carrier concentration $n$ with $x$ can be explained by the difference of film density induced by evolution of microstructure. It is noteworthy that the Hall mobility $\mu_H$ of thick films increased by 30% from 45.15 $cm^2 \cdot V^{-1} \cdot s^{-1}$ for $x$=6.5 to 58.85 $cm^2 \cdot V^{-1} \cdot s^{-1}$ for $x$=8. The enhancement of $\mu_H$ is attributed to the improved electrical contact between $Bi_{0.5}Sb_{1.5}Te_3$ powders. However, with $x$ further increasing, the Hall mobility decreased. This is due to the loose microstructure caused by relatively low content of

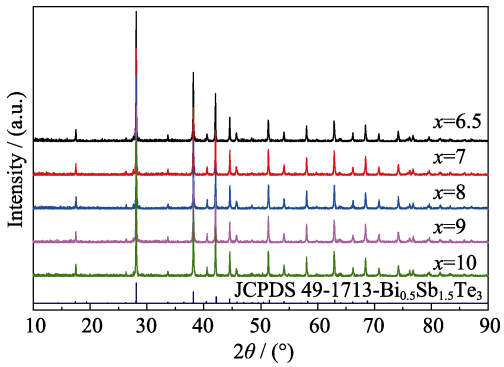


Fig. 1 XRD patterns of the composite films prepared with different contents of $Bi_{0.5}Sb_{1.5}Te_3$ powder

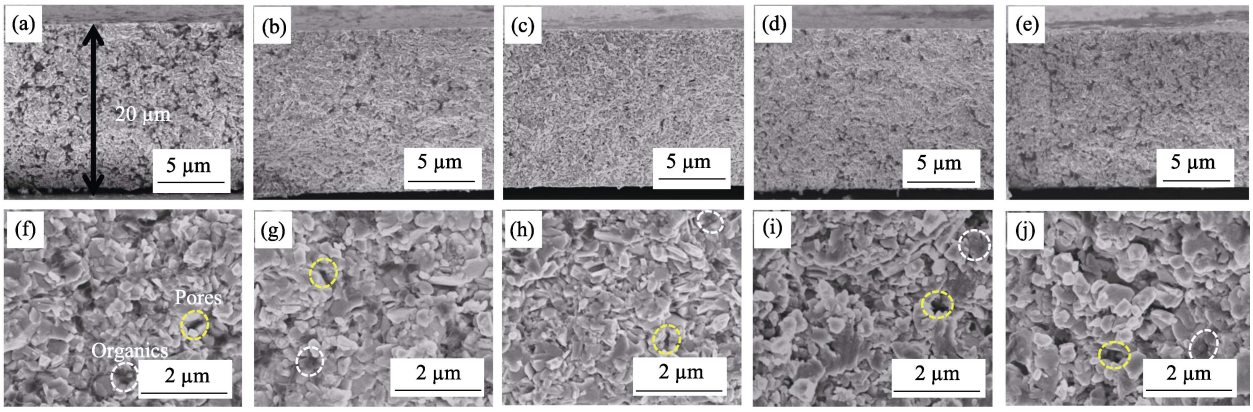


Fig. 2 Cross-sectional FESEM images of the composite thick films prepared with different contents of $Bi_{0.5}Sb_{1.5}Te_3$ powder
(a, f) $x$= 6.5; (b, g) $x$= 7; (c, h) $x$= 8; (d, i) $x$= 9; (e, j) $x$= 10

**Table 1 Densities and electrical properties of the composite films at room temperature**

| $x$ | $\rho$/(g·cm$^{-3}$) | $R_H$/(×10$^{-1}$, cm$^3$·C$^{-1}$) | $n$/(×10$^{19}$, cm$^{-3}$) | $\mu_H$/(cm$^2$·V$^{-1}$·s$^{-1}$) | $\sigma$/(×10$^4$, S·m$^{-1}$) |
|---|---|---|---|---|---|
| 6.5 | 3.93 | 3.72 | 1.67 | 45.15 | 1.21 |
| 7 | 4.08 | 3.69 | 1.69 | 52.17 | 1.41 |
| 8 | 4.32 | 3.57 | 1.74 | 58.85 | 1.65 |
| 9 | 4.19 | 3.56 | 1.73 | 54.69 | 1.51 |
| 10 | 4.05 | 3.55 | 1.72 | 50.59 | 1.40 |

epoxy resin. The variation trend of electrical conductivity $\sigma$ is consistent with $\mu_H$.

Fig. 3 shows the temperature dependence of electrical conductivity $\sigma$, Seebeck coefficient $\alpha$ and power factor $\alpha^2\sigma$ of these composite films. $\sigma$ decreased as the test temperature increases, similar with the metallic transport behavior of the bulk $Bi_{0.5}Sb_{1.5}Te_3$ materials[24]. It is worth noting that $\sigma$ increased significantly with the content of $Bi_{0.5}Sb_{1.5}Te_3$ powder, $x$ increasing from 6.5 to 8 and then decreased as the $x$ was further increased. The improved $\sigma$ can be explained by the reduced organics and improved grain contact as shown in Fig. 2, which led to greater mobility. When $x$ further increases, the amount of epoxy resin is not enough to effectively adhere the grains, which leads to loose microstructure. Obviously, the deteriorated microstructure must cause decreased $\mu_H$ and $\sigma$. As shown in Fig. 3(b), $\alpha$ almost remains constant with $x$ increasing. Thus, the power factor $\alpha^2\sigma$ increased significantly with the content of $Bi_{0.5}Sb_{1.5}Te_3$ powder, $x$ increasing from 6.5 to 8 and then decreased as the $x$ was further increased. When $x$=8, the optimized power factor of thick films reached 1.12 mW·m$^{-1}$·K$^{-2}$. Table 2 summarizes the electrical conductivity $\sigma$ and power factor $\alpha^2\sigma$ of $Bi_2Te_3$-based composite films in this work and literature[10,14,17,20,22,25]. As shown in Table 2, the optimized electrical conductivity and power factor of the as-prepared composite films are much higher than all of the reported composite films, showing increments of

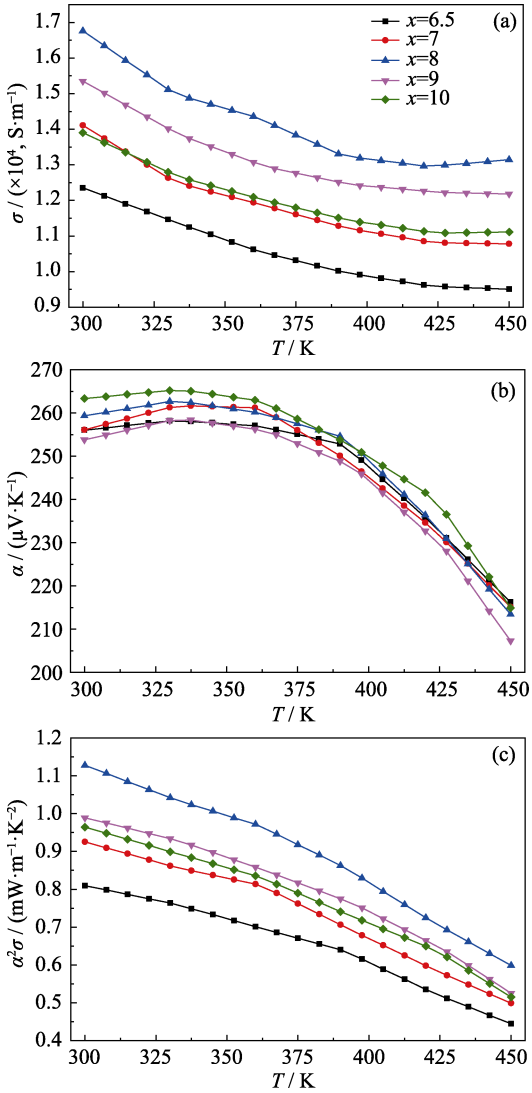


Fig. 3 Temperature dependence of (a) electrical conductivity $\sigma$, (b) Seebeck coefficient $\alpha$ and (c) power factor $\alpha^2\sigma$ of the composite thick films prepared with different content of $Bi_{0.5}Sb_{1.5}Te_3$ powder

33% and 331% as compared with the power factor of our previous work[22] and $Bi_2Te_3$+1%Se/epoxy composite films[20], respectively.

**Table 2 Comparison of $\sigma$ and $\alpha^2\sigma$ of $Bi_2Te_3$-based composite films reported by different groups**

| Materials | Fabrication process | Annealing methods | $\sigma/(\times10^4, S\cdot m^{-1})$ | $\alpha^2\sigma/(mW\cdot m^{-1}\cdot K^{-2})$ | Ref. |
|---|---|---|---|---|---|
| $Bi_{0.5}Sb_{1.5}Te_3$+epoxy | Screen printing | 573 K, 4 h, hot pressing | 1.67 | 1.12 | This work |
| $Bi_{0.5}Sb_{1.5}Te_3$ ink | Inkjet printing | 673 K, 30 min | 0.20 | 0.07 | [10] |
| $Bi_{0.5}Sb_{1.5}Te_3$+8%Te-epoxy | Dispenser printing | 523 K | 0.11 | 0.06 | [14] |
| $Bi_{0.5}Sb_{1.5}Te_3$+$C_{24}H_{44}O_6$ | Brush-printed | 673 K, 4 h | 0.29 | 0.15 | [17] |
| $Bi_2Te_3$+1%Se-epoxy | Dispenser printing | 623 K, 12 h | 1.03 | 0.26 | [20] |
| $Bi_{0.5}Sb_{1.5}Te_3$+epoxy | Brush-printed | 623 K, 4 h, hot pressing | 1.15 | 0.84 | [22] |
| $Bi_{0.5}Sb_{1.5}Te_3$+8%Te-polymer | Dispenser printing | 523 K | 0.13 | 0.16 | [25] |

Fig. 4 shows the variation rates of resistance ($\Delta R/R_0$) for the TE leg prepared by the optimal content of $Bi_{0.5}Sb_{1.5}Te_3$ powder before and after anti-bending tests with different bending radius and bending cycles. As shown in Fig. 4(a), the resistance variation rates are almost 0 when the bending radius gradually decreases from 90 mm to 20 mm, and rapidly increases when the bending radius is less than 10 mm. As shown in Fig. 4(b), the resistance variation rates are less than 5% within 3000 bending cycles when the bending radius is 20 mm. The anti-bending test results indicate the as-prepared films have potential application in flexible TE devices.

Fig. 5 shows the temperature distribution of the TE leg prepared by the optimal content of $Bi_{0.5}Sb_{1.5}Te_3$ powder. As shown in Fig. 5, the TE leg could establish a hot end and a cold end when applied different currents. The temperature difference ($\Delta T$) between the hot end ($T_h$) and cold end ($T_c$) increases from 4.2 ℃ to 7.8 ℃ with the current increasing from 0.01 A to 0.05 A, showing potential application in planar cooling field. However, both the temperatures of hot end and cold end gradually increases with the current increasing due to Joule heat effect induced by the internal resistance of the TE leg. According to the thermodynamic analysis of TE cooling device[26-27], there are several different effects for the thermal energy in the device, such as thermal energy from Peltier effect, thermal conduction energy from Fourier effect, and Joule thermal energy from the internal resistance of the device.

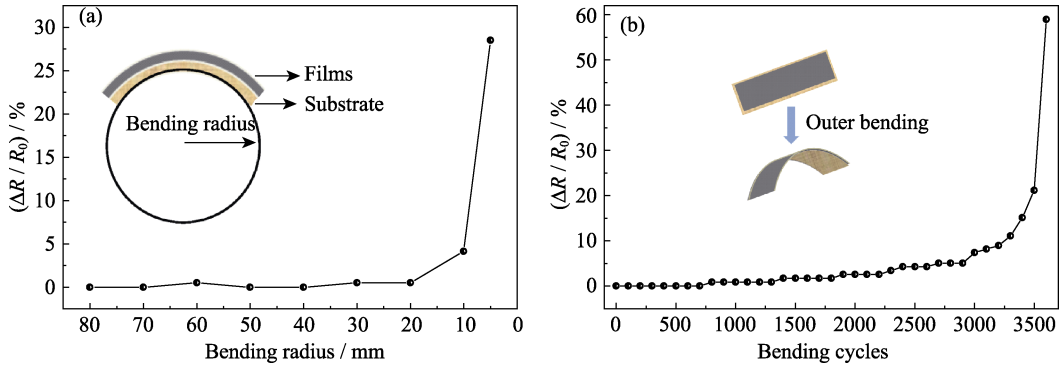


Fig. 4 Anti-bending tests of flexible films: (a) bending radius and (b) bending cycles

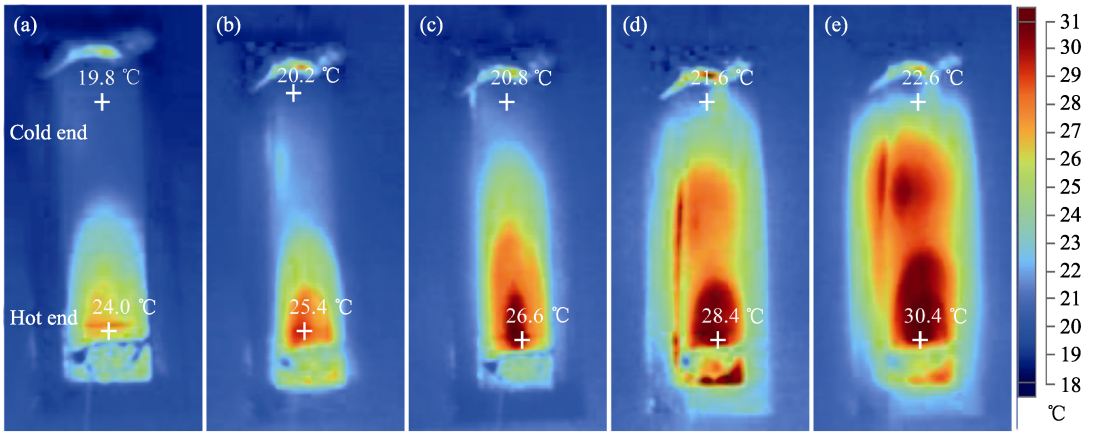


Fig. 5 Visual infrared images of the composite thick films measured with different currents ($I$)
(a) $I$=0.01 A; (b) $I$=0.02 A; (c) $I$=0.03 A; (d) $I$=0.04 A; (e) $I$=0.05 A

When the thermal energy from Peltier effect is greater than those from Fourier effect and Joule heat effect, $T_c$ decreases. Thus, the research in next step will focus on decrease of the internal resistance of TE legs and the device structure design.

# 3 Conclusions

A series of flexible $Bi_{0.5}Sb_{1.5}Te_3$/epoxy composite thermoelectric thick films were successfully prepared on polyimide substrates by screen printing. It is discovered that the content of $Bi_{0.5}Sb_{1.5}Te_3$ powder plays a vital role in improving the microstructure and electrical transport properties. The results indicate that as the content of $Bi_{0.5}Sb_{1.5}Te_3$ powder increases, the electrical conductivity firstly increases and then decreases with the Seebeck coefficient remaining almost constant, and the power factor follows the same trend as the electrical conductivity. The optimized power factor reaches 1.12 $mW \cdot K^{-2} \cdot m^{-1}$, increased by 33% as compared with our previous work. The anti-bending test indicates that the resistance of the thick films remains unchanged when the bending radius is over 20 mm and slightly increases within 3000 bending cycles when the bending radius is 20 mm, implying that the as-prepared films have potential application in flexible thermoelectric devices. The cooling performance of a single TE leg was evaluated by applying different current. A temperature difference from 4.2 to 7.8 ℃ was observed under working current from 0.01 A to 0.05 A, showing potential application in planar cooling field.

# Acknowledgments

XRD and FESEM experiments were performed at the Center for Materials Research and Testing of Wuhan University of Technology. The transport properties measurements were performed at State Key Lab of Advanced Technology for Materials Synthesis and Processing of Wuhan University of Technology.

## References:

[1] SIMONS R E, EllSWORTH M J, CHU R C. An assessment of module cooling enhancement with thermoelectric coolers. *J. Heat Transf*., 2005, **127(1):** 76–84.

[2] ZHANG H Y, MUI Y C, TARIN M. Analysis of thermoelectric cooler performance for high power electronic package. *Appl. Therm. Eng*., 2010, **30(6/7):** 561–568.

[3] AVRAM B C, IYENGAR M, KRAUS A D. Design of optimum plate-fin natural convective heat sinks. *J. Electronic Packag.*, 2003, **125(2):** 208–216.

[4] BELL L E. Cooling, heating, generating power, and recovering waste heat with thermoelectric systems. *Science*, 2008, **321(5895):** 1457–1461.

[5] HARMAN T C, TAYLOR P J, WALSH M P, *et al*. Quantum dot superlattice thermoelectric materials and devices. *Science*, 2002, **297(5590):** 2229–2232.

[6] CHOWDHURY I, PRASHER R, LOFGREE K, *et al*. On-chip cooling by superlattice-based thin-film thermoelectrics. *Nat. Nanotechnol.*, 2009, **4(4):** 235–238.

[7] HAO F, QIU P F, TANG Y S, *et al*. High efficiency $Bi_2Te_3$-based materials and devices for thermoelectric power generation between 100 and 300 ℃. *Energy & Environ Sci.*, 2016, **9(10):** 3120–3127.

[8] DISALVO F J. Thermoelectric cooling and power generation. *Science*, 1999, **285(5428):** 703–706.

[9] YANG J, STABLER F R. Automotive applications of thermoelectric materials. *J. Electron. Mater.*, 2009, **38(7):** 1245–1251.

[10] LU Z, LAYANI M, ZHAO X, *et al*. Fabrication of flexible thermoelectric thin film devices by inkjet printing. *Small*, 2014, **10(17):** 3551–3554.

[11] XU B, AGNE M T, FENG T L, *et al*. Nanocomposites from solution-synthesized PbTe-BiSbTe nanoheterostructure with unity figure of merit at low-medium temperatures (500–600 K). *Adv. Mater.*, 2017, **29(10):** 1605140–1–9.

[12] ZHU T J, HU L P, ZHAO X B, *et al*. New insight into intrinsic point defects in $V_2VI_3$ thermoelectric materials. *Adv. Sci.*, 2016, **3(7):** 1600004–1–16.

[13] MADAN D, CHEN A, WRIGHT P K, *et al*. Dispenser printed composite thermoelectric thick films for thermoelectric generator application. *J. Appl. Phys.*, 2011, **109(3):** 034904–1–6.

[14] MADAN D, WANG Z Q, CHEN A, *et al*. Dispenser printed circular thermoelectric devices using Bi and $Bi_{0.5}Sb_{1.5}Te_3$. *Appl. Phys. Lett.*, 2014, **104(1):** 013902–1–4.

[15] KIM S J, WE J H, CHO B J. A wearable thermoelectric generator fabricated on a glass fabric. *Energy & Environ Sci.*, 2014, **7(6):** 1959–1965.

[16] VARGHESE T, HOLLAR C, RICHARDSON J, *et al*. High-performance and flexible thermoelectric films by screen printing solution-processed nanoplate crystals. *Sci. Rep.*, 2016, **6(1):** 33135–1–6.

[17] WU H, LIU X, WEI P, *et al*. Fabrication and characterization of brush-printed p-type $Bi_{0.5}Sb_{1.5}Te_3$ thick films for thermoelectric cooling devices. *J. Electron. Mater.*, 2016, **46(5):** 2950–2957.

[18] SHI J X, CHEN H L, JIA S H, *et al*. Rapid and low-cost fabrication of thermoelectric composite using low-pressure cold pressing and thermocuring methods. *Mater. Lett.*, 2018, **212:** 299–302.

[19] CAO Z, KOUKHARENKO E, TUDOR M J, *et al*. Flexible screen printed thermoelectric generator with enhanced processes and materials. *Sens. Actuators A*, 2016, **238:** 196–206.

[20] MADAN D, WANG Z Q, CHEN A, *et al*. Enhanced performance of dispenser printed MA n-type $Bi_2Te_3$ composite thermoelectric generator. *ACS Appl. Mater. Inter.*, 2012, **4(11):** 6117–6124.

[21] MADAN D, WANG Z Q, CHEN A, *et al*. High-performance dispenser printed MA p-type $Bi_{0.5}Sb_{1.5}Te_3$ flexible thermoelectric generators for powering wireless sensor networks. *ACS Appl. Mater. Inter.*, 2013, **5(22):** 11872–11876.

[22] HOU W K, NIE X L, ZHAO W Y, *et al*. Fabrication and excellent performance of $Bi_{0.5}Sb_{1.5}Te_3$/epoxy flexible thermoelectric cooling devices. *Nano Energy*, 2018, **50:** 766–776.

[23] GUO X, JIA X, QIN J, *et al*. Fast preparation and high thermoelectric performance of the stable $Bi_{0.5}Sb_{1.5}Te_3$ bulk materials for different synthesis pressures. *Chem. Phys. Lett.*, 2014, **610:** 204–208.

[24] SUH D, LEE S, MUN H, *et al*. Enhanced thermoelectric performance of $Bi_{0.5}Sb_{1.5}Te_3$-expanded grapheme composites by simulta-

neous modulation of electronic and thermal carrier transport. *Nano Energy*, 2015, **13:** 67–76.
[25] MADAN D, WANG Z Q, WRIGHT P K, *et al*. Printed flexible thermoelectric generators for use on low levels of waste heat. *Appl. Energy*, 2015, **156:** 587–592.
[26] CHEN J C, YAN Z J, WU L Q. Nonequilibrium thermodynamic analysis of a thermoelectric device. *Energy*, 1997, **22(10):** 979–985.
[27] CHEN L G, WU C, SUN F R. Heat transfer effect on the specific cooling load of refrigerators. *Appl. Therm. Eng.*, 1996, **16(12):** 989–997.

# $Bi_{0.5}Sb_{1.5}Te_3$/环氧树脂柔性复合热电厚膜的制备及其面内制冷性能

李 鹏, 聂晓蕾, 田 烨, 方文兵, 魏 平, 朱婉婷, 孙志刚, 张清杰, 赵文俞

(武汉理工大学 材料复合新技术国家重点实验室, 武汉 430070)

**摘 要:** 利用丝网印刷法在聚酰亚胺基板上制备了 $Bi_{0.5}Sb_{1.5}Te_3$/环氧树脂柔性复合热电厚膜, 通过优化 $Bi_{0.5}Sb_{1.5}Te_3$ 粉末含量提高了其电输运性能。复合厚膜在 300 K 时的最优功率因子达到 1.12 $mW\cdot m^{-1}\cdot K^{-2}$, 较前期报道的数值提高了 33%。抗弯测试表明复合厚膜的电阻在弯曲半径大于 20 mm 时基本不变, 在弯曲半径为 20 mm, 弯曲次数小于 3000 次时, 仅有轻微增大, 说明其在柔性热电器件领域具有应用潜力。红外热成像技术显示, 在工作电流为 0.01 A 到 0.05 A 时, 复合厚膜热电臂两端可以形成 4.2 ℃到 7.8 ℃的温差, 表明了其在面内制冷领域应用的可能性。

**关 键 词:** 柔性热电厚膜; 丝网印刷法; $Bi_{0.5}Sb_{1.5}Te_3$/环氧树脂复合厚膜; 电输运性能; 面内制冷领域

**中图分类号:** TQ174 **文献标识码:** A